A Platinum Open Access Journal for Organic Chemistry

Paper

Free to Authors and Readers | DOAJ Seal | *Arkivoc* **2023** (vii) 202312069

Novel peptidomimetics: synthesis, characterization, and molecular modeling studies

Özgür Yılmaz*

Materials Technologies, Marmara Research Center, TUBITAK, 41470, Gebze, Kocaeli, Turkey
Email: yilmaz.ozgur@tubitak.gov.tr

Received 08-23-2023 **Accepted Manuscript** 10-10-2023 **Published on line** 10-17-2023

Abstract

Since PD-1/PD-L1 plays a crucial role as immune checkpoint molecules in many cancers, developing immunotherapy with peptidomimetics that block these molecules is an important option in anticancer therapy. In this study, several peptidomimetic compounds were screened from the literature using computational methods, and it was determined that 2-amino-benzothiazole-based peptidomimetics show affinity for the active site of PD-L1. In the light of molecular modelling studies, six molecules with free binding energies ranging from -6.7 to -7.2 kcal/mol were chosen from the library of 2-amino-benzothiazole-based peptidomimetics for synthesis. These synthesized six compounds were characterized with ^{1}H-NMR, ^{13}C-NMR, FTIR and HRMS. Molecular modelling studies showed that these novel 2-amino-benzothiazole-based peptidomimetics may be potential checkpoint inhibitors for cancer immunotherapy.

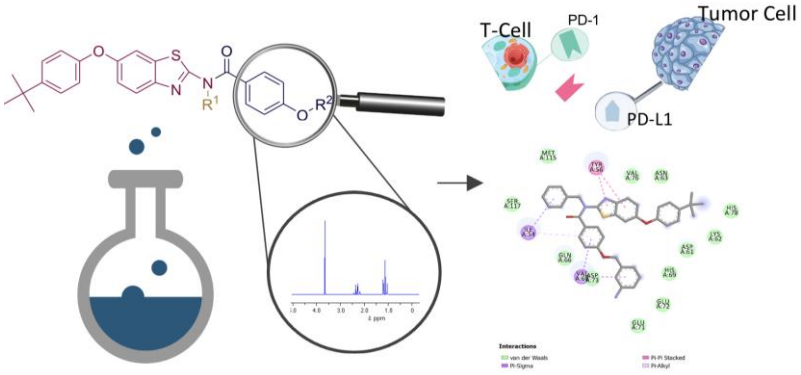

Keywords: Immunotherapy, PD-L1, PD-1, peptidomimetics, 2-aminobenzothiazole

Introduction

Immune checkpoint is a sort of signal to regulate the processes of T cells in immune responses. There are two types of signals based on antigen recognition by T cells; stimulatory signals to stimulate immune progression or inhibitory signals to suppress immune progression.

Programmed cell death 1 receptor (PD-1) and its ligand programmed cell death ligand 1 (PD-L1) are a type of inhibitory immune checkpoint molecules. PD-1 is found on the cell surface of T cells while PD-L1 is expressed in dendritic cells, T cells, B cells, macrophages, and cancer cells. When PD-1 receptor binds to its ligand PD-L1, the immune response of T-cells is supressed. Increased PD-L1 expression within the tumor microenvironment has been identified as a hindrance to the antitumoral T-cell response. Many experimental studies on PD-1 blockers confirmed that these molecules are clinically effective in various malignancies and proved that these inhibitors are promising anticancer agents.[1]

Immunotherapy, a type of anticancer treatment, involves the utilization of inhibitors that specifically target the interaction of immune checkpoint molecules. Immune checkpoint inhibitors used in immunotherapy can be in the form of peptide-based, non-peptide small molecule, or monoclonal antibodies (mAbs)2. In the context of immunotherapy, five mAbs targeting PD-1 (Nivolumab, Pembrolizumab) and PD-L1 (Atezolizumab, Avelumab, Durvalumab) have been approved by the FDA for use in anticancer therapy in the clinic.[3,4] Although immunotherapy based on mAbs targeting the PD-1/PD-L1 pathway offers unique clinical responses, these inhibitors have some limitations, such as high production costs, poor oral bioavailability, long half-life, poor tissue and tumor penetration.[5] The area where antibodies typically engage with proteins consists of peptide chains. The PD-1/PD-L1 features a partially flat and hydrophobic interaction surface which significantly constrains the development of novel inhibitors.[6] One of the approaches to overcome these challenges is the development of peptidomimetics as an alternative to mAbs.

Progress is currently being made in the development of small molecules, particularly peptidomimetics, that block PD-1/PD-L1.[7] Peptidomimetics are derived from the modification of peptide sequences by replacing the peptide backbone with a molecular scaffold to improve biological properties. Such compounds are designed to be highly stable, selective, and metabolically bioavailable. So, peptidomimetics appear to be an important tool for targeting protein-protein interactions such as immune checkpoint molecules in drug discovery studies. Consequently, in immunotherapy, the exploration of peptidomimetic compounds as potential antagonists to inhibit the PD-1/PDL-1 interaction is contemplated as an alternative approach.

The present study aims to design and synthesize novel peptidomimetic compounds directed towards the PD-1/PDL-1 pathway. Numerous peptidomimetic compounds were screened from the literature using computational methods, and it was determined that 2-amino-benzothiazole-based peptidomimetics (Figure 1) display a pronounced affinity for the active site of PD-L1. In the light of docking studies, a library of 2-amino-benzothiazole-based peptidomimetics was constructed, which are specific to PD-L1 and six of these compounds (**8a-b**, **9a-b** and **10a-b**) were chosen for synthesis. The six synthetic compounds were characterized with ^{1}H-NMR, ^{13}C-NMR, FTIR and HRMS.

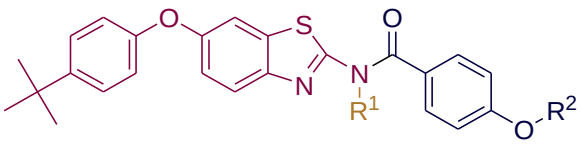

Figure 1. Novel 2-amino-benzothiazole-based peptidomimetic derivatives (**8a-b**, **9a-b** and **10a-b**).

Results and Discussion

Synthesis of peptidomimetics

Six novel peptidomimetics (**8a-b**, **9a-b**, and **10a-b**) were synthesized, derived from substituted acyl halides **7a-b**, 2-aminobenzothiazole **3**, and benzyl halides, as summarized in Table 1. Synthesis of new carrier compounds that can be used in anticancer imaging probes includes three main steps. The initial stage involves the synthesis of the 2-aminobenzothiazole derivative, as showcased in Scheme 1. Compound **1** was synthesized through a substitution reaction between 4-*tert*-butylphenol and 1-fluoro-4-nitrobenzene in a basic medium, resulting in a yield of 70-75%. Following this, intermediate **2** was obtained with a yield of 45-50% through the reduction of compound **1** in an acidic medium in the presence of $SnCl_2$. 2-Aminobenzothiazole **3** was synthesized through a bromine-catalyzed thiosination of intermediate **2**, with subsequent removal of impurities via precipitation in cold methanol.[8,9]

Table 1. Synthesized novel peptidomimetic compounds (**8a-b**, **9a-b** and **10a-b**)

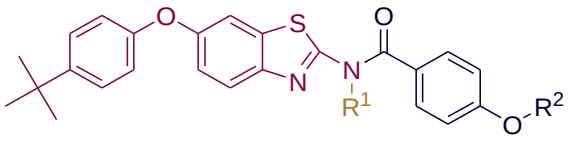

Comp No.	R^1	R^2	Yield %
8a	H	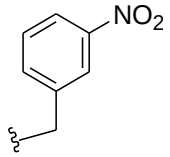	65
8b	H	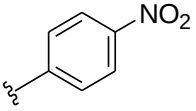	70
9a	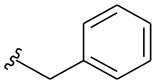	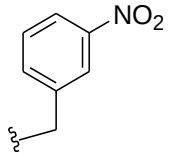	68
9b	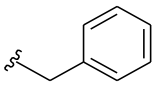	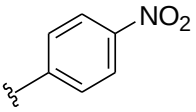	70
10a	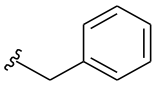	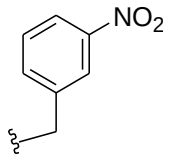	50
10b	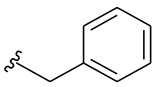	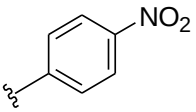	70

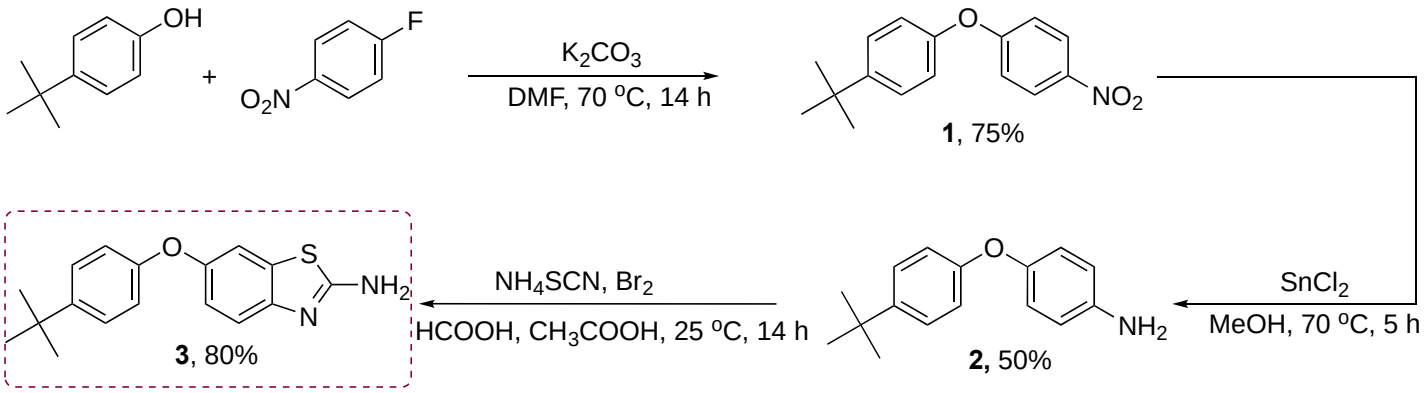

Scheme 1. Synthesis of the 2-aminobenzothiazole derivative.

In the second step, the synthesis of intermediates **5a-b** were achieved with 75-82% yield as a result of the substitution reaction of methyl 4-hydroxybenzoate and substituted benzylic halides **4a-b** in basic medium. Following this, substituted benzoic acid intermediates **6a-b** were obtained in high yields, ranging from 95% to 97%, as a result of basic hydrolysis of the ester groups. Substituted benzoic acid intermediates in the presence of diethylaminosulfide trifluoride (DAST) formed substituted benzoyl fluorides **7a-b** in good yields by nucleophilic fluoridation (Scheme 2). In this reaction, the disappearance of the OH band in the FTIR spectrum of compounds **7a-b** was accompanied by a noticeable shift in the frequency of the C=O group.

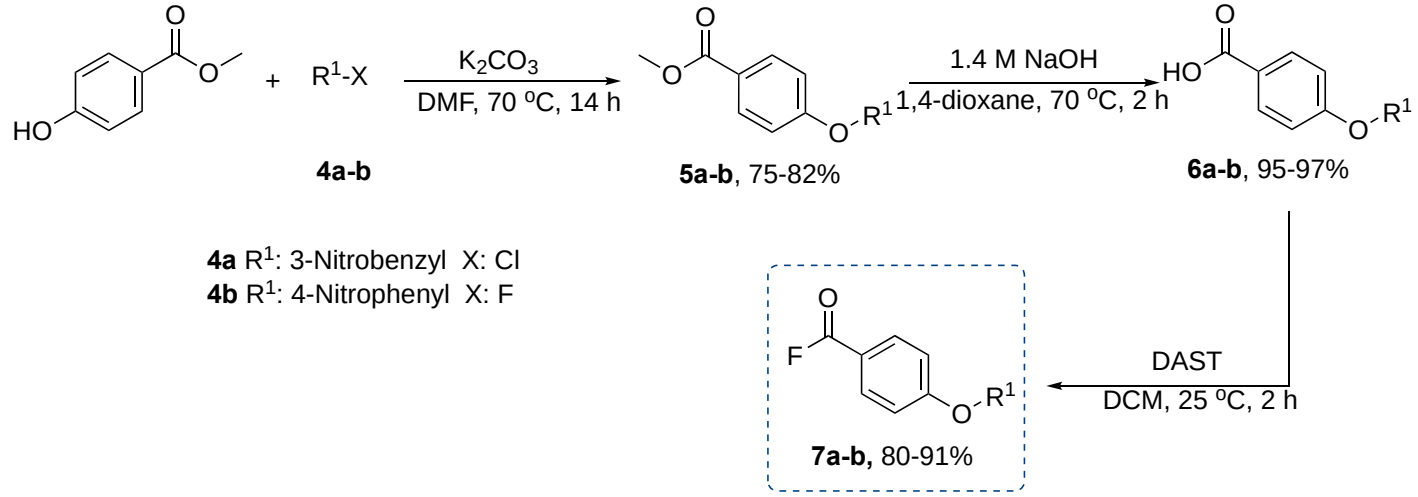

Scheme 2. Synthesis of the substituted benzoyl fluorides.

In the final step, the reaction of the intermediate 2-aminobenzothiazole derivatives with substituted benzoyl fluoride was carried out in the presence of diisopropylethylamine (DIPEA). The obtained compound **8a-b** was subjected to alkylation in a basic medium, resulting in the formation of compound **9a-b** with a yield of 68-70%. Two different methods were employed for the reduction of compound **9a-b** molecules. One of these methods involves $SnCl_2$-catalyzed reduction in the presence of acid, while the other involves Fe-catalyzed reduction. Accordingly, peptidomimetic compounds **10a** and **10b** were obtained with yields of 50% and 70%, respectively (Scheme 3).[10,11]

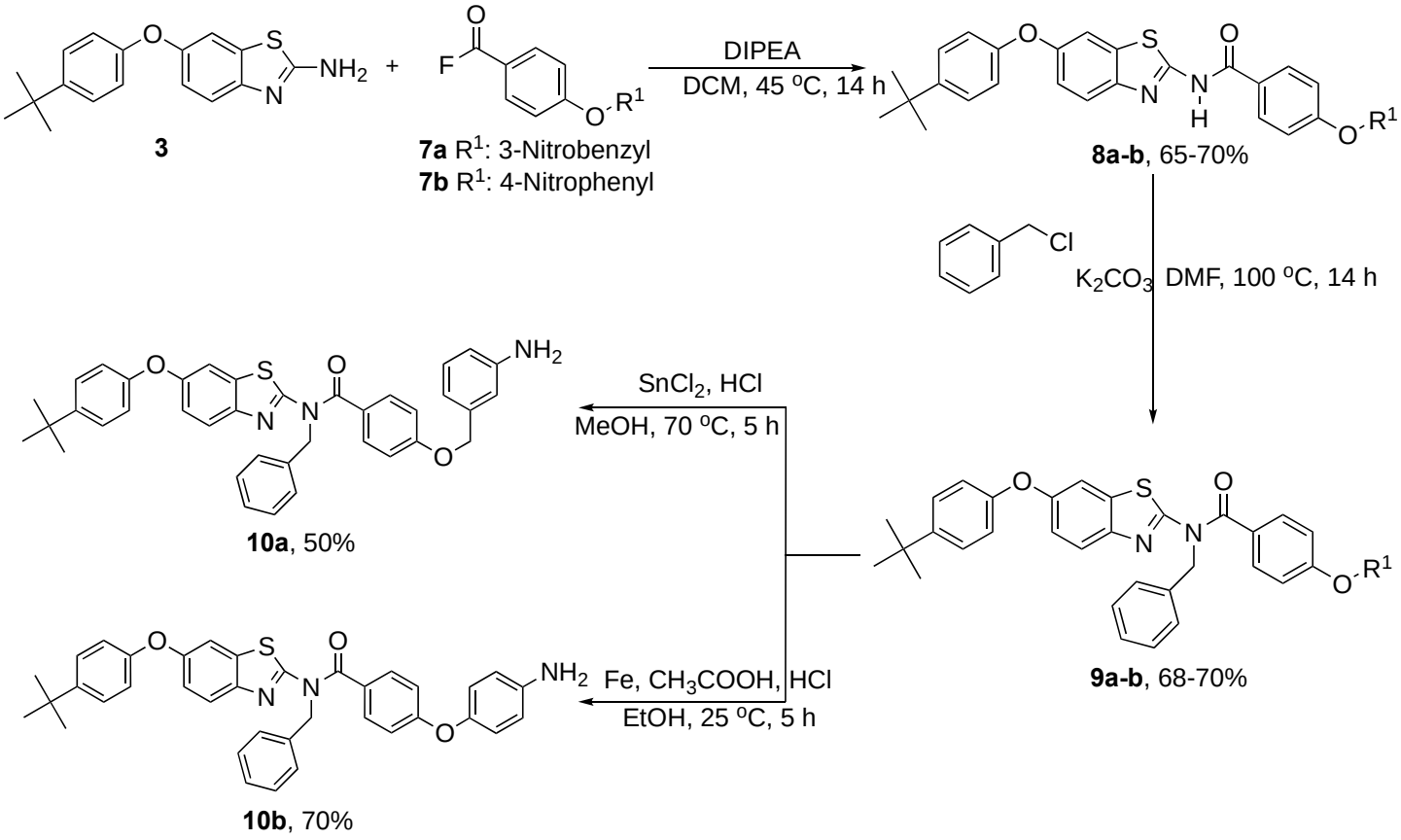

Scheme 3. Synthesis of novel peptidomimetic compounds.

Molecular docking studies

In molecular docking studies, the best binding affinity and receptor-ligand interaction of all compounds were evaluated. Good interactions of the newly synthesized peptidomimetic compounds within the target PD-L1 receptor active site are given in Table 2. Compounds **10a** and **9b** showed good binding affinity towards PD-L1 with free binding energies ΔG:-7.2 kcal/mol and -7.1 kcal/mol, respectively. The interaction diagrams of compounds **10a** and **9b** were shown in Figures 2 and 3. The best docking interactions of compounds **10a** and **9b** with the PD-L1 are shown in Figures 4 and 5.

Compound **10a** interacted with amino acids ILE A: 54 and VAL A: 68 via pi-sigma bonds with alkyl groups. On the other hand, π-π stacked interaction was observed with TYR A:56 amino acid via the benzothiazole ring. Moreover, compound **10a** implicated van der Waals interactions with MET A: 115, VAL A: 76, ASN A: 63, HIS A: 78, LYS A:62, ASP A: 61, HIS A:69, GLU A: 72, GLU A:71, ASP A:73, GLN A:66 and SER A: 117. Compound **9b** demonstrated a π-σ interaction with MET A:115, while also engaging in a π-alkyl interaction with the alkyl group of ALA A:12. In the 2D diagram of interactions between PD-L1 and **9b**, Van der Waals interactions were observed with SER A:117, ILE A:54, VAL A:68, GLN A:66, LYS A:62, ASN A:63, ASP A:61, VAL A:76, ASP A:122, TYR A:123 and ILE A:116. In addition to all these interactions, it forms a π-π bond with TYR A:56 amino acid.

Table 2. Structures and molecular docking scores for novel peptidomimetics

Comp. No	Structures	ΔG (Kcal/mol)
8a	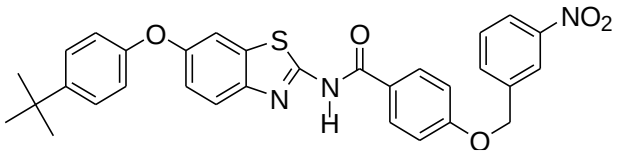	-6.7
8b	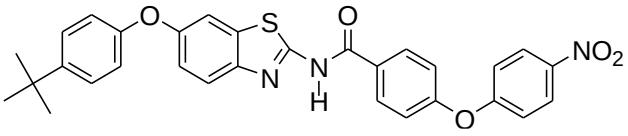	-6.7
9a	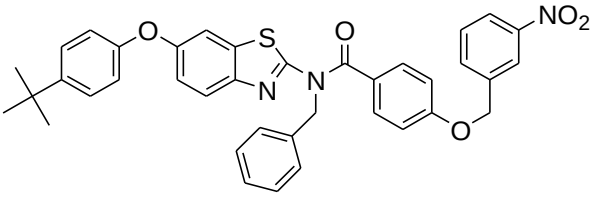	-7.1
9b	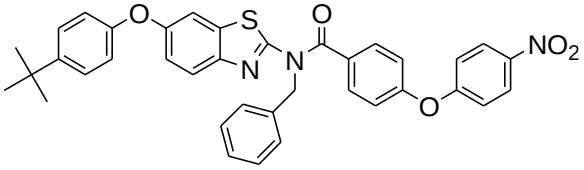	-7.1
10a	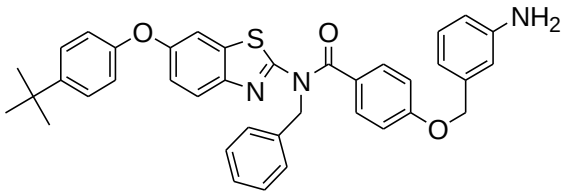	-7.2
10b	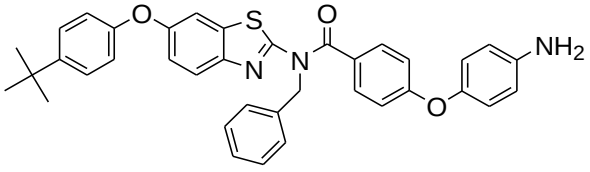	-6.8

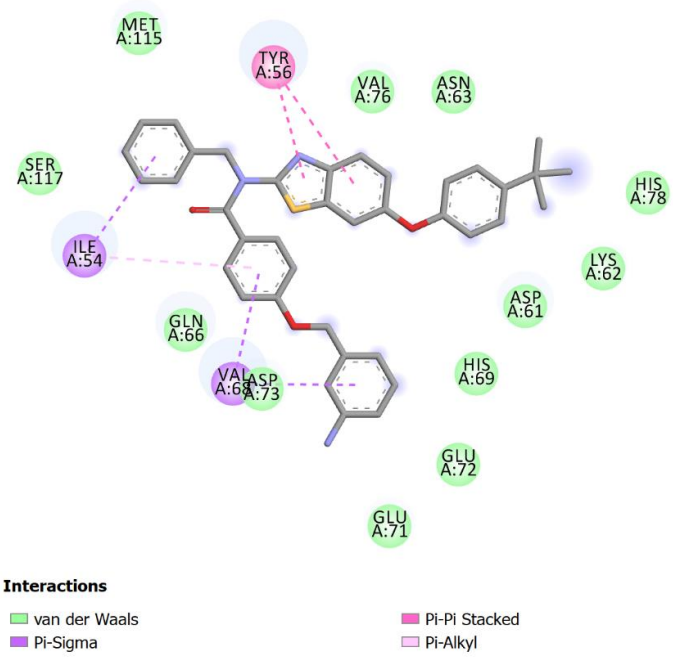

Figure 2. 2D diagram of interactions involved between PD-L1 and **10a**.

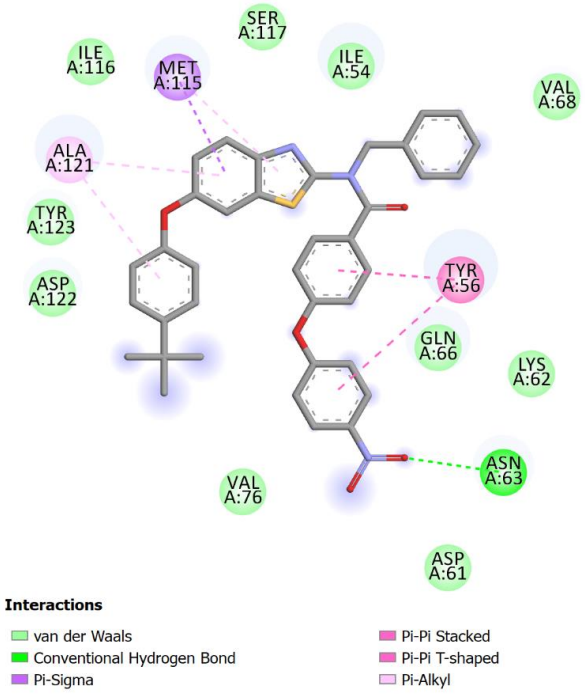

Figure 3. 2D diagram of interactions involved between PD-L1 and **9b**.

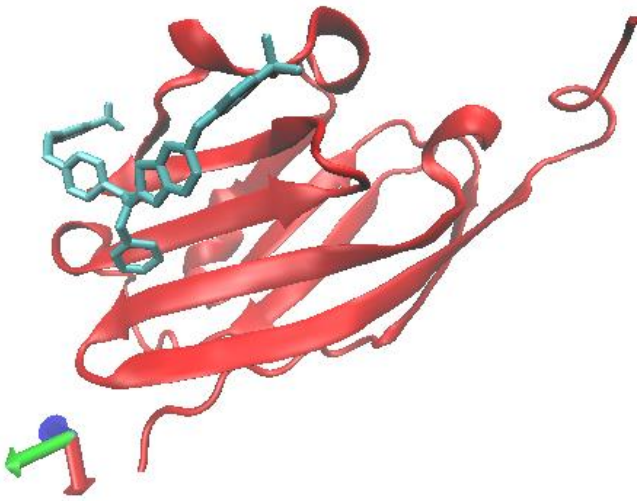

Figure 4. Interaction of best-docked pose of **10a** compound with PD-L1.

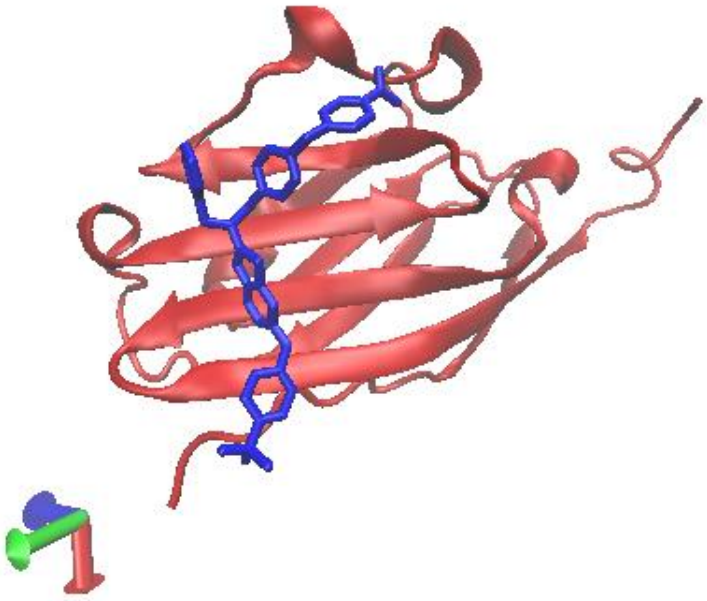

Figure 5. Interaction of best-docked pose of **9b** compound with PD-L1.

Molecular dynamic simulation

RMSD provides the information of structural stability of the proteins. The plots show PD-L1 receptor alone and its complex with the ligand **9b** and **10a** separately. All the systems show a stable state throughout the MD simulations. The RMSD of the PD-L1-**9b** complex and steadily increases from ~3 Å to ~5 Å and then stabilizes through the simulation. The RMSD of the PD-L1-**10a** complex also changes from ~3 Å to ~5 Å and then stabilized toward the end of the simulation. So, the PD-L1-**9b** complex shows a steady RMSD profile throughout the whole 200 ns simulation. As same, The RMSD of the PD-L1-**10a** complex rises from ~2.8 Å to ~4.8 Å, then finally stabilizing around 3 Å at the end of the simulation showing that **10a** is also a plausible inhibitor candidate for PD-L1 receptor.

The radius of gyration (Rg) measures the compactness of the protein in which also shows the stability of the inhibitors with its complexes. Rg profiles of the PD-L1 receptor alone and its complexes with the two hits (**9b** and **10a**) are plotted as shown in the figures (Figure 6). All the systems show low Rg trends in between 1.24 Å and 1.32 Å over 200 ns so that the protein kept stable throughout the simulation. This means that **9b** and **10a** are perfect inhibitor candidates for PD-L1 receptor.

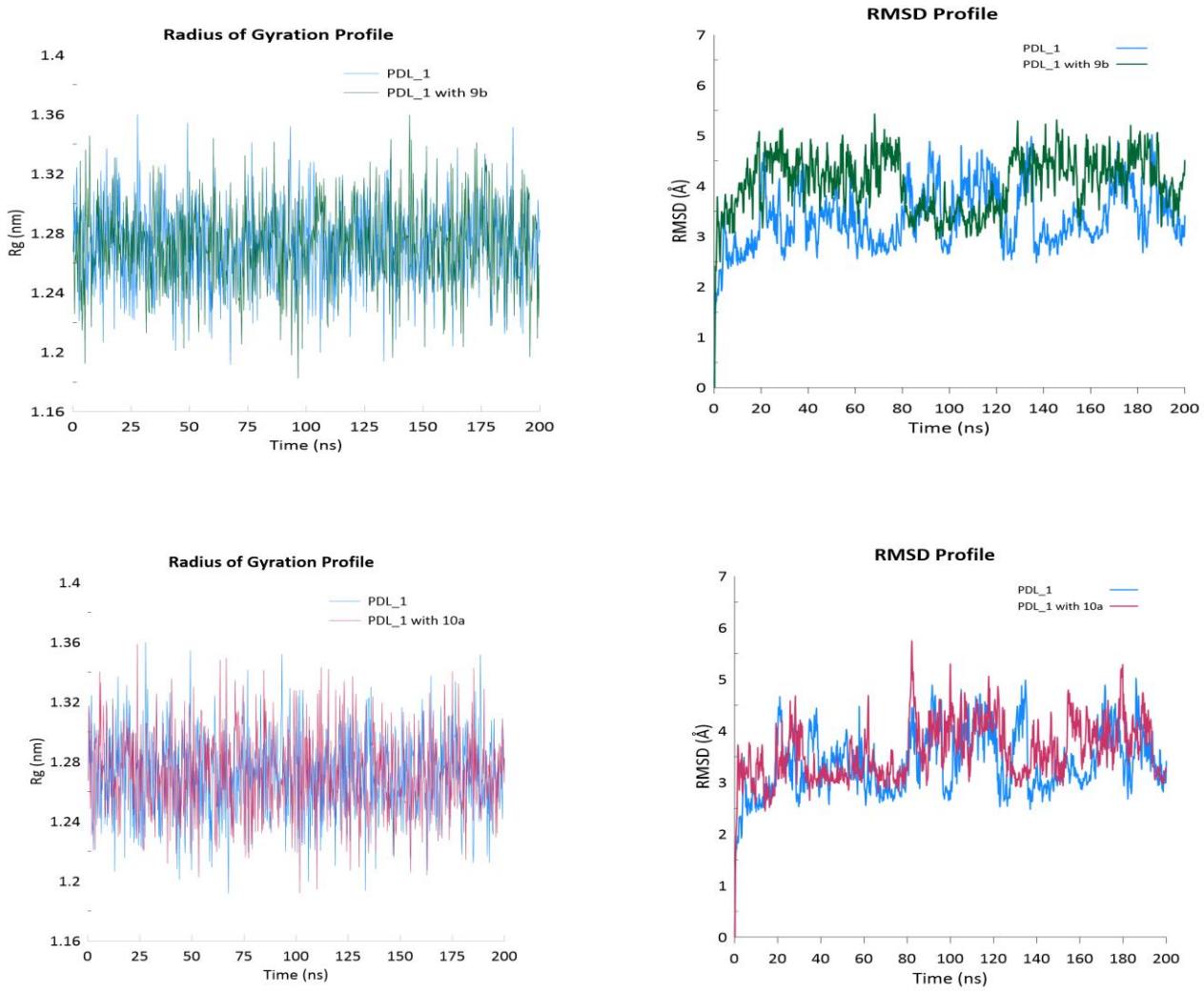

Figure 6. Root-mean-square deviation (RMSD) and radius of gyration (Rg) profiles displayed over 200 ns simulation of the PDl_1 receptor alone and its complexes with **9b** and **10a.**

Conclusions

In this study, six new 2-amino-benzothiazole-based peptidomimetics (8a-b, 9a-b, 10a-b) that could bind with high affinity to PDL1, which is known to be overexpressed on various cancer such as breast cancer, lung cancer, colorectal cancer, gastric cancer, hepatocellular carcinoma, renal cell carcinoma, esophageal cancer, pancreatic cancer, ovarian cancer, and bladder cancer, were identified through docking studies. Then, molecular docking simulations were performed for these compounds. RMSD and RG results were obtained for PD-L1 receptor-ligand complexes. These six peptidomimetics were synthesized, purified in high yield and

characterized by ^{1}H-NMR, ^{13}C-NMR, HRMS and FTIR. This study showed that, from an *in-silico* perspective, these peptidomimetics may be suitable candidates as immune checkpoint inhibitors for the PD-1/PD-L1 pathway. We conclude that these new peptidomimetics will give promising results in cancer treatment in the light of preclinical studies planned to be conducted in the future.

Experimental Section

General. All utilized chemicals and solvents were of analytical grade, sourced from commercial vendors (Merck, Sigma-Aldrich, Acros Organics) and used without further purification. The solvents employed in chromatography were of technical grade and underwent distillation prior to utilization. The compounds **1-3** and **5b-7b**, which were used as starting materials, were synthesized according to our previously published work.[12] ^{1}H NMR and ^{13}C NMR spectra were recorded at 500 MHz and 126 MHz, respectively. DMSO-d_6 was used as a solvent, and Me_4Si was used as the internal standard. FTIR spectra were recorded on a Perkin-Elmer FTIR System Spectrum BX (Massachusetts, USA) over the range 4000–500 cm^{-1} spectrophotometer. TLC spots were marked under UV light (254 nm, t = 25 °C). The synthesized compounds were characterized by an Agilent 6530 Q-TOF mass spectrometer equipped with an Electrospray Ionization (ESI) source.
Copies of NMR, MS and FTIR spectra of the synthesized compounds are given in the Supporting Information.

Chemistry

Preparation of 4-(3-nitro-benzyloxy)benzoic acid methyl ester (5a).[9] Methyl 4-hydroxybenzoate (1 equiv., 3.73 mmol), 3-nitrobenzyl chloride (1 equiv., 3.73 mmol) and K_2CO_3 (3 equiv., 11.19 mmol) were dissolved in DMF (10 mL) and a suspension reaction medium was obtained. The reaction mixture was stirred at 70 °C for 14 hours. At the end of the reaction, ethyl acetate (15 mL) was added and the reaction was washed with water (15 mL x 3) and brine (15 mL x 1). The organic phase was washed with distilled water (15 mL x 3) and brine (15 mL x 1), dried over anhydrous Na_2SO_4, and concentrated under reduced pressure. Yield: 82%.

4-(3-Nitrobenzyloxy)-benzoic acid methyl ester (5a). White powder, ^{1}H-NMR (500MHz, $CDCl_3$) δ ppm: 3.91 (3H, s); 5.23 (2H, s); 7.02 (2H, d, *J* = 8.7 Hz); 7.04 (1H, t, *J* 8.7 Hz); 7.21 (1H, d, *J* = 8.8 Hz); 7.60 (1H, t, *J* 7.9 Hz); 7.79 (1H, d, *J* 7.6 Hz); 8.04 (2H, d, *J* 8.8 Hz); 8.23 (1H, d, *J* 8.1 Hz); 8.34 (1H, s). FTIR (ATR) υ_{max} /cm^{-1}: 3027 (C-H, aryl), 2963-2950 (C-H, alkyl), 1637 (C=O), 1585 (C=C, aryl), 1550, 1504 (N-O), 1210 (C-O), 740 (CH, aryl). M.W: 287.08 $gmol^{-1}$.

Preparation of 4-(3-nitrobenzyloxy)benzoic acid (6a).[9] 4-(3-Nitro-benzyloxy)-benzoic acid methyl ester **5a** (2.63 mmol) was dissolved in 1,4-dioxane (30 mL). NaOH solution (2.75 mL of 1.4 M) was added dropwise and stirred for 2 hours at 70 °C. At the end of the reaction, the dioxane was removed under reduced pressure and the residue was acidified to pH 2 with HCl solution (1 M). The precipitate was separated by vacuum filtration. After washing with water, dried under vacuum. Yield: 95%.

4-(3-Nitrobenzyloxy)benzoic acid (6a). White powder, ^{1}H-NMR (500 MHz, $CDCl_3$) δ ppm: 5.35 (2H, s); 7.13 (2H, t, *J* 7.9 Hz); 7.71 (1H, t, *J* 7.9 Hz); 7.95 (2H, d, *J* 8.2 Hz); 7.88 (2H, d, *J* 8.8 Hz); 8.21 (1H, d, *J* 8.1 Hz); 8.33 (1H, s); 12.66 (1H, s). FTIR (ATR) υ_{max} /cm^{-1}: 3302 (OH), 3022 (C-H, aryl), 2960 and 2867 (C-H, alkyl), 1620 (C=O), 1542 (C=C, aryl), 1530, 1513 (N-O), 1278 (C-O), 722 (CH, aryl). M.W: 273.06 $gmol^{-1}$.

Preparation of 4-(3-nitrobenzyloxy)benzoyl fluoride (7a).[8] 4-(3-Nitro-benzyloxy)-benzoic acid **6a** (1 equiv., 1.82 mmol) was dissolved in DCM (25 mL) under nitrogen conditions. DAST (4 equiv., 7.28mmol) was added in a 0°C ice bath and stirred at rt for 2 hours. At the end of the reaction, the mixture was extracted with ice water

(25 mL x 3) and DCM (25 mL x 3). After washing with saturated $NaHCO_3$, dried with $MgSO_4$, and concentrated under reduced pressure. Yield: 91%.

4-(3-Nitrobenzyloxy)benzoyl fluoride (7a). Yellow powder,^{1}H-NMR (500 MHz, DMSO-d_6) δ ppm: 8.32 (1H, s); 8.18 (1H, d, *J* 8.2 Hz); 7.99 (2H, d, *J* 7.9 Hz); 7.90 (1H, d, *J* 7.9 Hz); 7.69 (1H, t, *J* 7.7 Hz); 7.25 (2H, d, *J* 7.2 Hz); 5.39 (2H, s). FTIR (ATR) υ_{max} /cm^{-1}: 3018 (C-H, aryl), 2989 and 2843 (C-H, alkyl), 1637 (C=O), 1521 (C=C, aryl), 1544, 1511 (N-O), 1257 (C-O), 743 (CH, aryl). M.W: 275.06 gmol^{-1}.

General procedure for the synthesis of (8a-b).[10] Acyl fluoride (**7a-b**) (1 equiv., 0.17 mmol) and 6-(4-*tert*-butyl-phenoxy)-benzothiazol-2-ylamine **3** (1 equiv., 0.17 mmol) were dissolved in DCM (10 mL) under nitrogen. DIPEA (4 equiv., 0.68 mmol) was added and the reaction was stirred for 14 hours at 45 °C. The reaction mixture was allowed to cool down to rt and washed with 10% citric acid (2×20 mL), distilled water (2×20 mL), and saturated $NaHCO_3$ (2×20 mL), respectively. The organic phase was dried over Na_2SO_4 and the solvent was evaporated under reduced pressure. The product was washed with cold methanol and dried under vacuum. Yield: 65-70%.

***N*-[6-(4-*t*-Butylphenoxy)benzothiazol-2-yl]-4-(3-nitrobenzyloxy)benzamide (8a).** Yellow Powder, ^{1}H-NMR (500 MHz, DMSO-d_6) δ ppm: 8.33 (1H, s); 8.20 (1H, d, *J* 8.7 Hz); 8.13 (2H, d, *J* 7.6 Hz); 7.93 (1H, d, *J* 8.7 Hz); 7.72 (2H, d, *J* 8.7 Hz); 7.70 (1H, s); 7.38 (2H, d, *J* 7.8 Hz); 7.19 (2H, d, *J* 8.7 Hz); 7.11 (2H, s); 6.93 (2H, d *J* 8.7 Hz); 5.72 (1H, s); 5.37 (2H, s); 1.26 (9H, s). ^{13}C-NMR (126 MHz, DMSO-d_6) δ ppm: 167.3; 165.6; 162.2; 155.7; 153.3; 148.2; 146.5; 145.7; 139.3; 134.5; 131.7; 131.2; 131.0; 130.5; 129.9; 127.2; 123.4; 122.5; 118.8; 118.1; 125.2; 112.0; 68.8; 34.5; 34.4; 31.9. FTIR (ATR) υ_{max} /cm^{-1}: 3072 (NH), 3013 (C-H, aryl), 2925 and 2867 (C-H, alkyl), 1730 (C=O), 1545 (C=C, aryl), 1532, 1509 (N-O), 1234 (C-O), 765 (CH, aryl). HRMS (EI$^+$) (*m/z*): 554.50648 [M+H]; calcd for $C_{31}H_{27}N_3O_5S$: 554.6378 [M+H]$^+$.

***N*-[6-(4-*t*-Butylphenoxy)benzothiazol-2-yl]-4-(4-nitrophenoxy)benzamide (8b)**. Yellow Powder, ^{1}H-NMR (DMSO-d_6) δ ppm: 12.87 (1H, s); 8.12 (2H, d, *J* 9.4 Hz); 7.76 (1H, d, *J* 8.6 Hz); 7.68 (1H, s); 7.63 (2H, t, *J* 9.6 Hz); 7.56 (2H, t, *J* 8.6 Hz); 7.38 (4H, m); 7.14 (1H, d, *J* 9.6 Hz, *J* = 8.9 Hz); 6.94 (2H, d, *J* 7.6 Hz); 1.25 (9H, s). ^{13}C-NMR (126 MHz, DMSO-d_6) δ ppm: 174.0; 165.9; 157.4; 148.3; 139.7; 136.6; 134.3; 134.0; 131.6; 130.4; 129.5; 129.3; 128.8; 128.3; 127.8; 123.0; 122.2; 121.3; 120.9; 120.7; 115.6; 114.5; 112.5; 36.6; 29.9. FTIR (ATR) υ_{max} /cm^{-1}: 3455 (NH), 3074 (C-H, aryl), 2920 and 2866 (C-H, alkyl), 1739 (C=O), 1550 (C=C, aryl), 1676, (N-O), 1189 (C-O), 730 (CH, aryl). HRMS (EI$^+$) (*m/z*): 540.52323 [M+H]; calcd for $C_{30}H_{25}N_3O_5S$: 540.6112 [M+H]$^+$.

General procedure for the synthesis of 9a-b.[10] Benzyl halide (2 equiv., 0.32 mmol), the corresponding intermediate **8a-b** (1 equiv., 0.16 mmol) and K_2CO_3 (3 equiv., 0.48 mmol) were dissolved in DMF (10 mL) under nitrogen conditions. The reaction was stirred for 14 hours at 100 °C. At the end of the reaction, the mixture was extracted with DCM (20 mL x 3) and ice water (20 mL x 3). The organic phase was dried over Na_2SO_4 and the solvent was evaporated under reduced pressure. The product was washed with cold methanol and dried under vacuum. Yield: 68-70%.

***N*-Benzyl-*N*-[6-(4-*t*-butyl-phenoxy)benzothiazol-2-yl]-4-(3-nitro-benzyloxy) benzamide (9a)**. Yellow powder, ^{1}H-NMR (500 MHz, DMSO-d_6) δ ppm: 8.31 (1H, s); 8.21 (3H, m); 7.92 (1H, d, *J* 8.7 Hz); 7.69 (1H, t, *J* 7.9 Hz); 7.63 (2H, d, *J* 7.6 Hz); 7.41 (2H, d, *J* 8.7 Hz); 7.37 (2H, d, *J* 8.6 Hz); 7.32 (2H, t, *J* 7.7 Hz); 7.25 (1H, t, *J* 7.8 Hz); 7.13 (3H, m); 6.92 (2H, d, *J* 7.8 Hz); 5.79 (2H, s); 5.34 (2H, s); 1.25 (9H, s). ^{13}C-NMR (126 MHz, DMSO-d_6) δ ppm: 173.4, 167.8, 162.4, 159.5, 158.3, 157.5, 154.1, 153.5, 143.3, 142.1, 133.3, 132.5, 132.1, 130.9, 130.3, 129.9, 129.5, 129.3, 127.9, 127.1, 120.8, 120.2, 119.3, 118.8, 118.8, 113.6, 112.1, 62.4, 57.0, 35.3, 28.2. FTIR (ATR) υ_{max} /cm^{-1}: 3025 (C-H, aryl), 2919 and 2877 (C-H, alkyl), 1643 (C=O), 1503 (C=C, aryl), 1566 (N-O), 1598 (C=N), 1128 (C-O), 740 (CH, aryl). HRMS (EI$^+$) (*m/z*): 644.21951 [M+H]; calcd for $C_{38}H_{33}N_3O_5S$: 644.2223 [M+H]$^+$.

***N*-Benzyl-*N*-[6-(4-*t*-butylphenoxy)benzothiazol-2-yl]-4-(4-nitrophenoxy)benzamide (9b).** Yellow powder, ^{1}H-NMR (DMSO-d_6) δ ppm: 8.34 (2H, d, *J* 9.1 Hz); 8.26 (2H, d, *J* 7.0 Hz); 7.66 (1H, d, *J* 9.6 Hz, *J* 8.8 Hz); 7.64 (1H, t, *J*

7.7 Hz); 7.40 (2H, s); 7.38 (2H, d, *J* 8.7 Hz); 7.31 (3H, t, *J* 7.3 Hz); 7.26 (2H, d, *J* 7.3 Hz); 7.22 (2H, d, *J* 8.7 Hz); 6.93 (2H, d, *J* 8.8 Hz, *J* = 8.6 Hz); 5.81 (2H, s); 1.25 (9H, s). ^{13}C-NMR (126 MHz, DMSO-d_6) δ ppm: 173.2, 167.8, 162.4, 159.7, 158.1, 157.7, 154.2, 153.5, 143.3, 137.5, 133.4, 132.8, 132.1, 129.8, 129.7, 127.9, 120.8, 120.1, 119.4, 118.8, 117.1, 117.0, 113.5, 57.7, 37.5, 29.7. FTIR (ATR) υ_{max} /cm^{-1}: 3028 (C-H, aryl), 2917 and 2866 (C-H, alkyl), 1738 (C=O), 1569 (C=C, aryl), 1566 (N-O), 1548 (C=N), 1240 (C-O), 720 (CH, aryl). HRMS (EI$^+$) (*m/z*): 630.29110 [M+H]; calcd for $C_{37}H_{31}N_3O_5S$: 630.2067 [M+H]$^+$.

Procedure for the synthesis of 10a.[11] The corresponding intermediate **9a** (1 equiv., 0.15 mmol) was dissolved in methanol (20 mL). $SnCl_2$ (4 equiv., 0.6 mmol) was dissolved in HCl (37%, 5 mL) and added dropwise to the reaction medium. The reaction was stirred for 5 hours at 70 °C. At the end of the reaction, the methanol was evaporated under reduced pressure. The precipitate was dissolved in distilled water and the pH of the solution was brought to 11 with 1% NaOH solution. The resulting suspension mixture was precipitated by centrifugation, extracted with DCM (30 mL x 3) and distilled water (30 mL x 3). The organic phase was dried over Na_2SO_4 and the solvent was evaporated under reduced pressure. The product was washed with cold methanol and dried under vacuum. Yield: 50%.

4-(3-Aminobenzyloxy)-*N*-benzyl-*N*-[6-(4-*t*-butylphenoxy)benzothiazol-2-yl] benzamide (10a). White powder, ^{1}H-NMR (500 MHz, DMSO-d_6) δ ppm: 8.25 (2H, d, *J* 8.7 Hz); 7.99 (1H, d, *J* 7.5 Hz); 7.93 (2H, d, *J* 6.5 Hz); 7.67 (2H, d, *J* 8.9 Hz); 7.55 (7H, m); 7.43 (1H, d, *J* 7.3 Hz); 7.38 (1H, d, *J* 8.6 Hz); 7.33 (2H, d, *J* 7.4 Hz); 6.69 (1H, d, *J* 7.9 Hz); 5.82 (2H, s); 4.01 (2H, s); 1.25 (9H, s). ^{13}C-NMR (126 MHz, DMSO-d_6): δ 173.7; 168.5; 166.9; 156.1; 155.1; 150.3; 136.5; 134.8; 134; 133.6; 132.4; 132.3; 132.0; 129.2; 129.0; 128.6; 127.9; 123.6; 123.5; 123.3; 120.8; 118.1; 115.6; 114.0; 112.5; 112.2; 62.4; 55.0; 34.8; 26.9. FTIR (ATR) υ_{max} /cm^{-1}: 3345 (NH), 3031 (C-H, aryl), 2955 and 2829 (C-H, alkyl), 1728 (C=O), 1550 (C=C, aryl), 1548 (C=N), 1212 (C-O), 754 (CH, aryl). HRMS (EI$^+$) (*m/z*): 614.43123 [M+H]; calcd for $C_{38}H_{35}N_3O_3S$: 614.2420 [M+H]$^+$.

Procedure for the synthesis of 10b. The corresponding intermediate **9b** (0.15 mmol) was dissolved in ethanol (10 mL) and acetic acid (10 mL). HCl (37%, 1 mL) and Fe powder (9 mmol) were added into the mixture. The reaction was then continued in an ultrasonic bath at rt. At the end of the reaction, the ethanol was evaporated under reduced pressure. The pH of the mixture was brought to 11 with 1% NaOH solution, extracted with DCM (30 mL x 3) and distilled water (30 mL x 3). The organic phase was dried over Na_2SO_4 and the solvent was evaporated under reduced pressure. The product was washed with cold methanol and dried under vacuum. Yield: 70%.

4-(4-Aminophenoxy)-*N*-benzyl-*N*-[6-(4-*t*-butyl-phenoxy)benzothiazol-2-yl]-benzamide (10b). White powder, ^{1}H-NMR (500 MHz, DMSO-d_6) δ ppm: 8.24 (2H, d, *J* 7.1 Hz); 7.92 (2H, d, *J* 6.7 Hz); 7.66 (1H, s); 7.59 (1H, t, *J* 5.8 Hz); 7.49 (4H, d, *J* 5.5 Hz); 7.41 (2H, d, *J* 7.4 Hz); 7.36 (2H, d, *J* 6.9 Hz); 7.32 (2H, d, *J* 6.1 Hz); 7.26 (1H, d, *J* 6.9 Hz); 7.14 (1H, d, *J* 8.5 Hz); 6.93 (2H, d, *J* 7.9 Hz); 5.82 (2H, s); 4.01 (2H, s); 1.25 (2H, s). ^{13}C-NMR (126 MHz, DMSO-d_6) δ ppm: 174.2; 173.4; 167.7; 162.7; 155.1; 153.9; 146.0; 136.5; 135.3; 133.45; 133.4; 129.6; 129.5; 129.45; 129.4; 129.3; 128.9; 128.3; 127.9; 127.2; 119.1; 118.3; 113.7; 34.4; 30.5; 28.5. FTIR (ATR) υ_{max} /cm^{-1}: 3356 (NH), 3028 (C-H, aryl), 2952 and 2851 (C-H, alkyl), 1755 (C=O), 1548 (C=C, aryl), 1538 (C=N), 1267 (C-O), 734 (CH, aryl). HRMS (EI$^+$) (*m/z*): 600.50471 [M+H]; calcd for $C_{37}H_{33}N_3O_3S$: 600.7420 [M+H]$^+$.

Molecular docking

PD-L1 is a crucial protein targeted in colorectal and breast cancer microenvironments in docking studies.[13] Structural Bioinformatics Research Collaboration (RCSB) Protein Data Bank was used for the selection of the targeted receptor and the 5j80 coded receptor was preferred.[14] In receptors crystal structure, PD-L1 and its inhibitor were observed as a complex. Docking processes were carried out between the relevant pdb-coded receptors and the candidate inhibitors synthesized, and the region where the inhibitor in the receptor complex binds was used as the binding site.[15] Candidate molecules were drawn with the ChemDraw program

and optimized in Biovia DS Studio 4.5 to prepare the receptor and candidate ligands for docking.[16] Candidate ligands are denoted by codes **8a-b**, **9a-b** and **10a-b** AutoDock Vina program was used in docking studies.[17] The center coordinates of the created grid box were determined as x, y and z, and the active region coordinates with a volume of 30x15x20 were selected and molecular docking was performed (Table 2). **10a** and **9b** with the best docking results were determined and visualized in Visual Molecular Dynamics (VMD) (Figure 4-5) and 2D interaction maps were made with Biovia DS Studio 4.5 program (Figure 2-3).[18]

Acknowledgements

The authors would like to thank the Turkish Scientific and Technological Council (project numbers: TUBITAK-116E661) for financial support.

Supplementary Material

FTIR, HRMS, ^{1}H-NMR and ^{13}C-NMR spectra of all target products, 2D Diagrams of interactions involved molecular docking.

References

1. Sun, C.; Mezzadra, R.; Schumacher, T. N. *Immunity* **2018**, *48*, 434-452. http://doi.org/10.1016/j.immuni.2018.03.014
2. Jia, L.; Zhang, Q.; Zhang, R. *Cancer Biol. Med.* **2018**, *5*,116-123. http://doi.org/10.20892/j.issn.2095-3941.2017.0086
3. Weber, J. *Semin. Oncol*. **2010**, *37*, 430-439. http://doi.org/10.1053/j.seminoncol.2010.09.005
4. Pardoll, D. M. *Nat. Rev. Cancer,* **2012**, *12*, 252-264. http://doi.org/10.1038/nrc3239
5. Cai, S.; Yang, X.; Chen, P.; Liu, X.; Zhou, J.; Zhang, H. *Bioorg. Chem*. **2020**, *94*, 103356. http://doi.org/10.1016/j.bioorg.2019.103356
6. Zarganes-Tzitzikas, T.; Konstantinidou, M.; Gao. Y.; Krzemien, D.; Zak, K.; Dubin, G.; Holak, T. A.; Dömling, A. *Expert. Opin. Ther. Pat*., **2016**, *26*, 973-977. http://doi.org/10.1080/13543776.2016.1206527
7. Guzik, K.; Tomala, M.; Muszak, D.; Konieczny, M.; Hec, A.; Błaszkiewicz, U.; Pustuła, M.; Butera, R.; Dömling, A.; Holak, T. A. *Molecules*, **2019**, *24*, 2071. http://doi.org/10.3390/molecules24112071
8. Baell, J. B.; Duggan, P. J.; Forsyth, S. A.; Lewis, R. J; Lok, Y. P; Schroeder, C. I. *Bioorg. Med. Chem*., **2004**, *12*, *15*, 4025-4037. http://doi.org/10.1016/j.bmc.2004.05.040
9. Yang, L.; Liu, W.; Mei, H., Zhang, Y.; Yu, X.; Xu, Y.; Li, H.; Huang, J.; Zhao, Z., *Med. Chem. Comm*. **2015**, *6, 4*, 671–676. http://doi.org/10.1039/C4MD00498A

10. Huang, S.; Hsei, I.; Chen, C. *Bioorg. Med. Chem.,* **2006**, *14, 17*, 6106–6119. http://doi.org/10.1016/j.bmc.2006.05.007
11. Korich, A. L.; Hughes, T. *Synlett* **2007**, *16*, 2602-2604. http://doi.org/10.1055/s-2007-986668
12. Köse, C., Uysal, E., Yazıcı, B., Tuğay, Z., Birgül, S., İ., D., Yanık, H., Tavukçuoğlu, E., Gülyüz, S., Akdemir, A., Esendağlı, G.; Yılmaz, Ö.; Alptürk, O. *Org. Commun*., **2020**, *13*, 89-102. http://doi.org/10.26434/chemrxiv.12936827.v1
13. Dou, D.; Ren, X.; Han, M.; Xu, X.; Ge, X.; Gu, Y; Wang, X. *Front. Immunol.* **2020**, *11*, 2026. http://doi.org/10.3389/fimmu.2020.02026
14. PCSB Protein data bank, RCSB PDB is funded by the National Science Foundation, DBI-1832184.
15. Amaral, M.; Kokh, D. B.; Bomke, J.; Wegener, A.; Buchstaller, H. P.; Eggenweiler, H. M.; Matias, P.; Sirrenberg, C.; Wade, R.; Frech, M. *Nat. Commun.* **2017**, *8*, 2276. http://doi.org/10.1038/s41467-017-02258-w
16. BIOVIA, D., S., BIOVIA Discovery Studio 2017 R2: A comprehensive predictive science application for the Life Sciences, In San Diego, CA, (USA) **2017**.
17. Trott, O; Olson, A. *J. Comput. Chem*., **2010**, *31, 2*, 455-461. http://doi.org/10.1002/jcc.21334
18. Humphrey, W.; Dalke, A.; Schulten, K. *J. Mol. Graph.* **1996**, *14, 1*, 33-38 http://doi.org/10.1016/0263-7855(96)00018-5